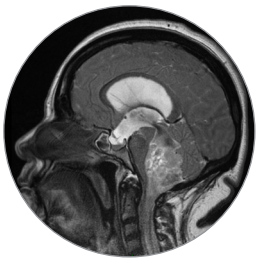

Differential Diagnosis of Fourth Ventricular Lesions

Diagnóstico diferencial de las lesiones del IV ventrículo

Katiuska Casares[1]
Ana Teresa Araújo[2]
Carlos Andrés Arias Durán[2]

Summary

The pediatric population is by far the most affected by lesions of the fourth (IV) ventricle. The vast majority present a similar radiological pattern, for which today, with the diffusion sequences, spectroscopy and ADC maps, it can be inferred that the visualized findings are more likely compatible with some of the pathologies that we will review later.

Key words (MeSH)

Medulloblastoma
Astrocytoma
Ependymoma
Hemangioblastoma

Resumen

La población pediátrica es, de lejos, la más afectada por las lesiones del cuarto (IV) ventrículo. La gran mayoría presentan un patrón radiológico similar; actualmente, con las secuencias de difusión, espectroscopia y mapas de ADC, se puede inferir la compatibilidad de los hallazgos visualizados con alguna de las patologías que se revisarán en el presente trabajo.

Palabras clave (DeCS)

Meduloblastoma
Astrocitoma
Ependimoma
Hemangioblastoma

1. Introduction

Lesions involving the fourth ventricle are more frequent in the pediatric population and the most common are medulloblastoma, pilocytic astrocytoma and ependymoma; in adults the most frequent are hemangioblastoma, subependymoma and metastases. Many of these lesions have a similar pattern in terms of density or intensity and enhancement, therefore, one should try to obtain a differential diagnosis as accurately as possible, using clinical and demographic data and imaging findings.

The IV ventricle is a cerebrospinal fluid (CSF) cavity that is continued upward by the aqueduct of Sylvius and opens downward and laterally to the subarachnoid space through the foramina of Luschkay Magendie. It has an anteroinferior wall or floor, consisting of the pons and bulb, and a postero superior wall or roof, which ends in a point at the level of the fastigium or posterior recess, consisting of the cerebellum and the posterior choroid tissue (1).

The fourth ventricle, like the rest of the ventricular system, is lined by ependymal cell epithelium and subependymal glial cells, and contains choroid plexuses which are the vascularized structures responsible for CSF production (1).

Lesions that may occupy the IV ventricle are classified into two main types depending on their origin. Primary lesions are derived from the ependymal epithelium, subependymal epithelium, choroid plexus and arachnoid tissue. Secondary lesions are paraventricular lesions with exophytic growth causing ventricular invasion (2).

Primary lesions include those originating from the choroid plexus, such as papilloma and carcinoma of the choroid plexus, meningiomas and metastases. Lesions originating from the ventricle wall include ependymoma and subependymoma (3). Non-neoplastic processes located within the fourth ventricle include neurocysticercosis and tuberculomas.

Secondary or extraventricular lesions with exophytic growth and intraventricular component include two thirds of intraaxial lesions, such as medulloblastoma, hemangioblastoma and astrocytomapillocytic (4, 5).

2. Lesion classification

2.1. Primary lesions

2.1.1. Papilloma and carcinoma of choroid plexuses

Choroid plexus tumors are primary tumors of the central nervous system of neuroepithelial origin. Their approximate annual incidence is estimated at 0.3 × 1,000,000 inhabitants. They account for 2-4% of pediatric brain tumors (20% in the first year of life) and 0.5% of all adult brain tumors (4). The more caudal the tumor, the older the age of onset, with a mean age of onset of 1.5 years in the lateral ventricles and III ventricle, and 22.5 years in the IV ventricle (6, 7). The World Health Organization (WHO) divides choroid plexus tumors into 3 types, with their corresponding grades: choroid plexus papilloma (CPP) WHO Grade I; atypical or anaplastic choroid plexus papilloma, WHO Grade II; and choroid plexus carcinoma (CPC) WHO Grade III. Atypical papillomas are characterized

[1]Neuroradiologist, Instituto Neurologia y Neuroradiologia Manuel Velasco Suárez. Bucaramanga, Colombia.

[2]Radiologist, Universidad Autónoma de Bucaramanga. Bucaramanga, Colombia.

by histology similar to choroid plexus papillomas, but with increased mitotic activity, with at least 2 or more mitoses in 10 high magnification fields. Choroid plexus carcinomas have 5 or more mitoses in 10 fields. The prognosis for patients with PPC is good, with a 5-year survival rate of 97%, but in CPC this rate is reduced to 26-43% (3, 4, 8).

These patients present with hydrocephalus as a result of increased CSF production by the neoplasm, direct obstruction to cerebrospinal fluid flow and decreased reabsorption due to protein exudate and hemorrhage affecting the arachnoid villi (4).

Imaging findings

These intraventricular lesions show well-defined contours, cauliflower shape, are very vascularized, so hemorrhages and cysts are common. Although histological grades cannot be differentiated histologically, papillomas and atypical papillomas have a lobulated appearance; choroid plexus carcinomas tend to have a more irregular contour, are heterogeneous due to necrosis and invade more the brain parenchyma (9-11).

In computed tomography (CT) they are observed as intraventricular lesions of medium or high density, which may have calcifications and areas of hemorrhage, and they enhance avidly with contrast medium (Figure 2).

In magnetic resonance imaging (MRI), a medium or low signal tissue is observed in the PPC in sequences with T1 information, medium or high signal in sequences with T2 information and with common signal voids due to flow (9). Periventricular vasogenic edema and intense homogeneous enhancement due to high vascularization can be observed. They do not show signs of water diffusion restriction. In perfusion sequences they reflect high arterial flow, which does not return to baseline due to loss of the blood-brain barrier, with persistence of contrast medium in the interstitium (4, 9, 12).

The spectroscopy sequence shows an elevated choline (Cho) peak and absence of the N-acetyl-aspartate (NAA) peak. CPCs show elevated lactate peak due to increased cell proliferation and anaerobic glycolysis. Some authors report increased myoinositol peak in papillomas as opposed to carcinomas (2, 9, 11, 13-15) (Figures 1 and 2).

2.1.2. Ependymoma

It represents 2-5% of intracranial neoplasms in adults (16), but it is the third most frequent posterior fossa tumor in children after pilocytic astrocytoma and medulloblastoma, with a mean age of presentation of 6 years. It is a glial tumor arising from the ependymal cells of the ventricular wall and medullary ependyma (4, 16, 17).

According to the WHO classification it is divided into grade I papillary ependymomyxoma, grade II ependymoma, grade II-III RELA-positive fusion ependymoma and grade III anaplastic ependymoma. Supratentorial ependymomas have a worse prognosis and higher relapse rates than those located in the posterior fossa (8, 18-20).

Imaging findings

Ependymomas originating in the IV ventricle tend to fill the ventricle and take its shape, and may extend through the foramen of Luschka or Magendie or the foramen magnum. It is common to observe a cystic component and irregular areas of calcification, and eventually areas of intratumoral hemorrhage (12, 17).

In CT ependymomas show medium or low density and in MRI they have medium to low signal in sequences with T1 information and medium to high signal in sequences with T2 information. There may be vasogenic edema in the periventricular white matter. They have heterogeneous enhancement with contrast medium, as well as foci of absence of signal due to calcification or hemorrhage in magnetic susceptibility sequences (3, 4) (figure 3).

In diffusion its signal is variable, depending on the cellularity of the tumor, with generally intermediate values of the apparent diffusion coefficient (ADC) (11, 21). In spectroscopy ependymomas have a neoplastic pattern with reduced NAA peak and moderate elevation of lactate and choline. In some cases they present high myoinositol (mI) and glycine (Gly) peaks with relative preservation of the NAA peak. However, spectroscopy alone does not differentiate them from other tumors (9, 11, 21-23).

In the perfusion sequence, ependymomas demonstrate markedly elevated cerebral blood volume and, unlike other glial tumors, have poor return to baseline due to alteration of the blood-brain barrier (11, 22) (Figure 3).

2.1.3. Subependymoma

They represent 0.7% of intracranial neoplasms. Most of these lesions appear in the IV ventricle (50-60%). They arise from the subependymal glial layer surrounding the ventricles. They predominate in males 2:1, and 82% occur in patients older than 15 years. The prognosis is good and recurrence after surgical resection is rare (2, 3, 12, 24).

Only one third of patients have clinical manifestations, especially those originating from the floor of the fourth ventricle, secondary to CSF flow obstruction. The most frequent clinical manifestations are headache, vomiting, dizziness and vertigo (25), and less frequently with focal neurological deficits and seizures (26). Subependymomas are WHO grade I neoplasms (8).

Imaging findings

Subependymomas are well-circumscribed, small lesions, less than 2 cm in diameter. They may show cystic degeneration, calcification or intratumoral hemorrhage. Unlike ependymomas, there is usually no extraventricular invasion (4, 11, 25).

In CT they are observed as low to medium density, intraventricular masses with well-defined contours. In MRI they are lesions of low to medium signal in sequences with T1 information, of high signal with T2 and FLAIR information, without edema of the adjacent parenchyma, and they can express foci of absence of signal by calcification or hemorrhage in sequences of magnetic susceptibility. Most lesions have little or no enhancement since they are avascular tumors (3, 11, 24) (Figure 4).

Subependymomas show greater free diffusion than the adjacent parenchyma, they have high signal in ADC maps. In perfusion studies they show very low cerebral blood volume, in spectroscopy sequences they show a normal choline peak and decreased NAA. Rarely, they show an increase in the choline/creatine ratio (27).

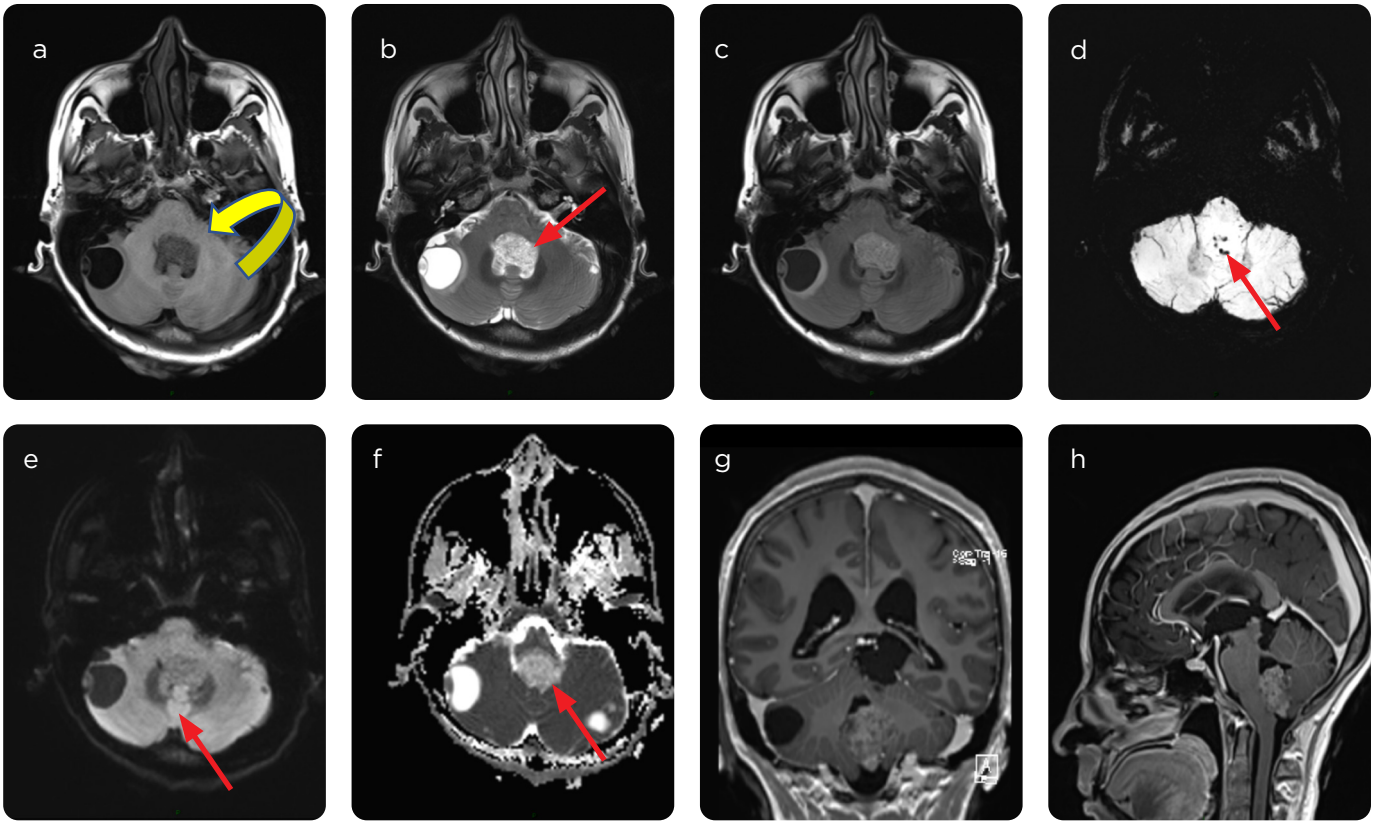

Figure 1. Papilloma of the IV ventricle MRI. a) Sequence with T1 information: low signal. b) Spin echo sequence; and c) FLAIR sequence with T2 information: high signal. d) Magnetic susceptibility sequence; low signal attributed to calcium. e) Diffusion sequence and f) ADC map: no restriction to water diffusion. g and h) With contrast medium: heterogeneous enhancement attributed to calcium.

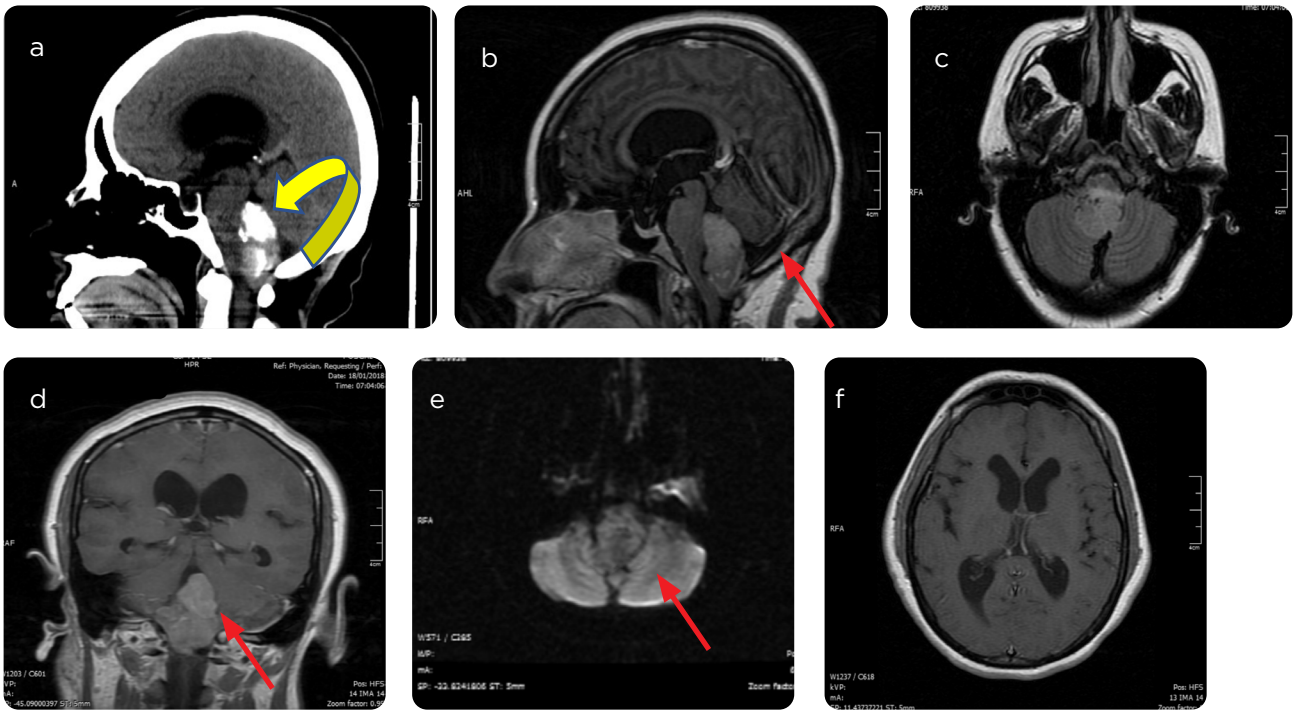

Figure 2. Carcinoma of the choroid plexus of the IV ventricle. a) CT scan: heterogeneous density with areas isodense to the parenchyma and calcifications. b) MRI with T1 information: isointense to the brain parenchyma. c) Sequences with T2 information of intermediate to high signal. d) With contrast medium: enhancement. e) Diffusion sequence: no restriction to water diffusion. f) Supratentorial axial image: dilatation of the ventricular system.

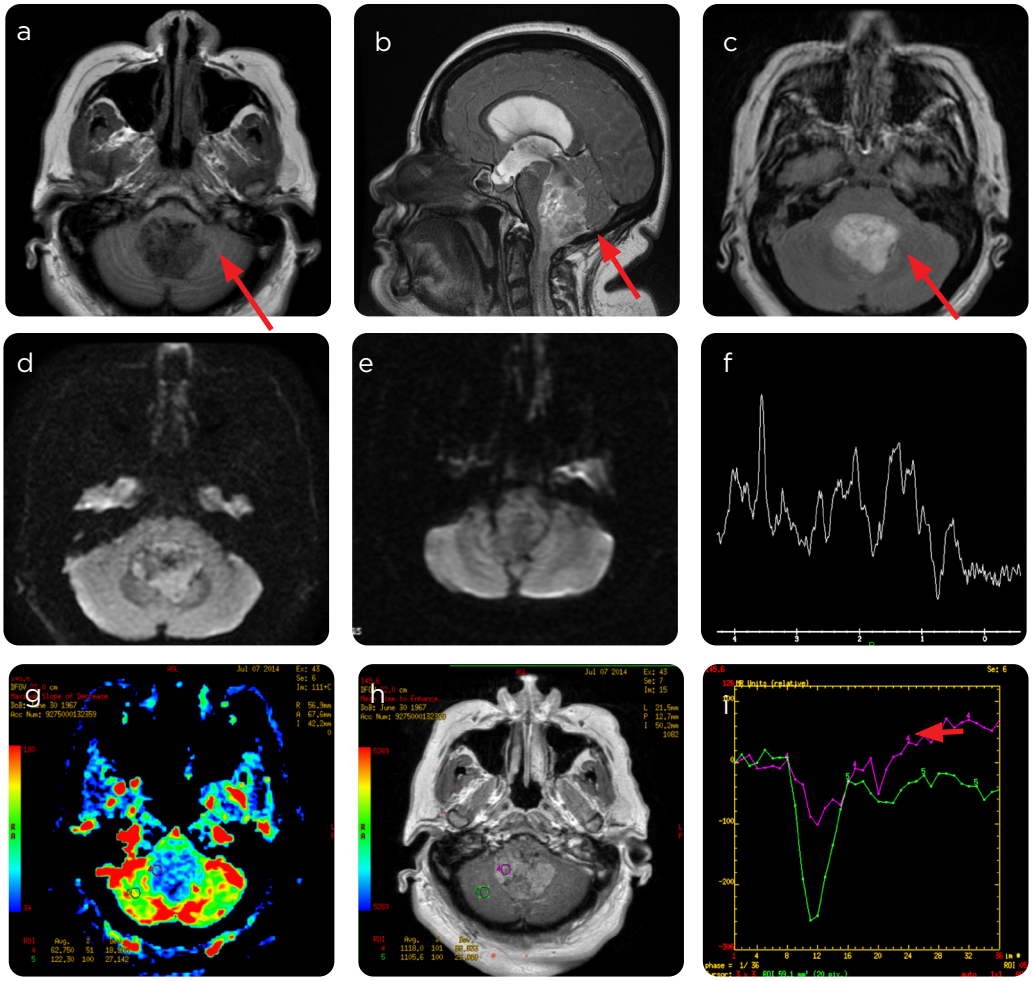

Figure 3. Ependymoma in the IV ventricle. a) Axial MRI sequence with T1 information, low to intermediate signal. b) With contrast medium: intense enhancement and discreetly heterogeneous. c) Sequence with T2 information: predominantly high signal. d) Diffusion sequence: intermediate signal. e and f) Perfusion: high cerebral blood volume without return to baseline.

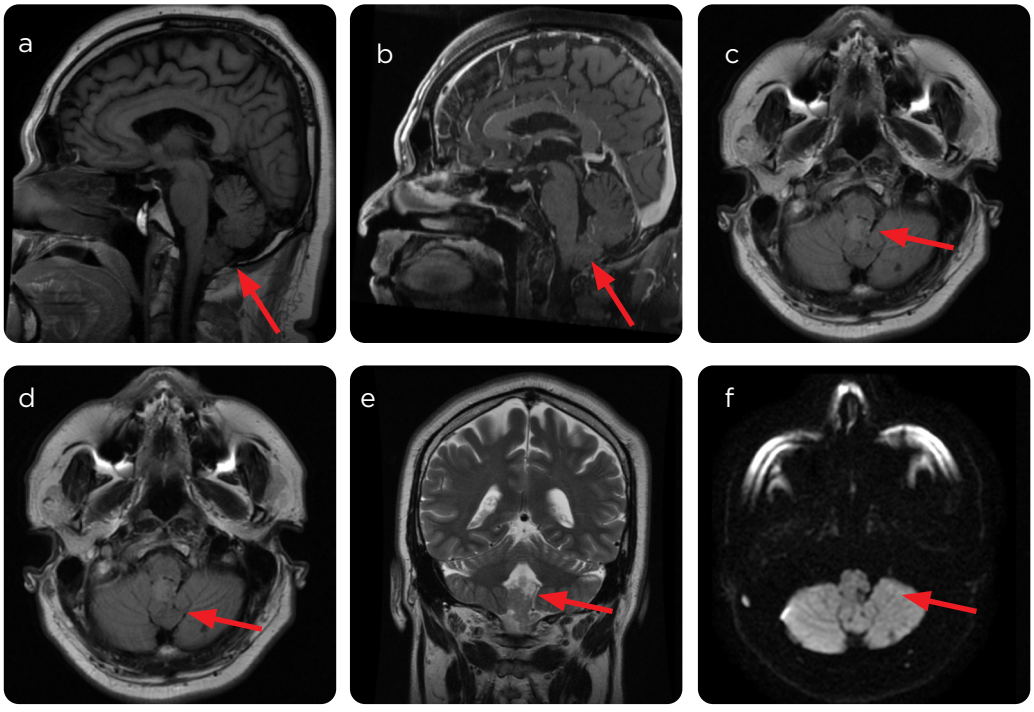

Figure 4. Subependymoma of the inferior medullary leaflet of the fourth ventricle. a) MRI with T1 information: intermediate signal lesion. b) With contrast medium: low enhancement. c and d) FLAIR sequence; and e) Spin echo with T2 information: discreetly high signal. e) Diffusion sequence: no restriction to water diffusion.

2.1.4. Meningiomas

Intraventricular meningiomas account for 0.5-3.7% of intracranial meningiomas. They arise from arachnoid cells trapped in the choroid plexus or choroid tissue during embryological formation of the choroid fissure and plexus. Of intraventricular meningiomas 77.8% occur in the lateral ventricles, 15.6% in the third ventricle and 6.6% in the fourth ventricle (2, 11, 28, 29). These slow-growing neoplasms usually reach large sizes before showing symptoms, which are intracranial hypertension, contralateral sensory or motor deficit and may also present intraventricular hemorrhage (3, 29).

Imaging findings

Meningiomas are well-circumscribed lesions of regular contours, they can be calcified (50%) and have cystic areas. In CT they are observed with medium or high density in reference to brain tissue; in MRI they are of low to medium signal in T1-weighted images, of medium to high signal in T2, they can show periventricular edema secondary to reabsorption of subependymal CSF or to the secretion of vascular endothelial growth factor by the meningioma (3, 4, 29).

They are highly vascularized and enhance intensely with contrast medium. In diffusion sequences they may show reduced diffusion velocity due to high cell density (9, 30-32).

In perfusion sequences, meningiomas show elevation of cerebral blood volume, with persistence of contrast material in the tumor interstitium due to the lack of a blood-brain barrier (2, 11, 27, 33).

In spectroscopy sequences the choline level is elevated, with variable amounts of lactate and lipids. An alanine peak, when present, can be useful in its diagnosis (doublet centered at 1.47ppm). As it is a mesenchymal lesion without neuronal tissue, it does not show NAA peak (4, 9, 11, 22).

2.2. Secondary lesions

2.2.1. Medulloblastoma

It is the most frequent malignant posterior fossa brain tumor in children, representing 20-25% of brain tumors in pediatrics and 40% of posterior fossa tumors. It is a WHO grade IV embryonal invasive tumor, with an inherent tendency to metastasize to the craniospinal axis, through the subarachnoid space (11-43%), on which its prognosis depends. The mean age of debut is 5-7 years (12, 34, 35). Histologically, according to the WHO 2016 review, they are classified into: classic (65-85 %), desmoplastic-nodular (15-25 %) and with extensive nodularity (5 %), and anaplastic/large cell (4-5 %). With the advent of molecular medicine it has been classified into 4 genetic groups. The Wnt/B-catenin (WNT) group is the least common (10%) and the one with the best prognosis, with a 5-year survival of 94%, which generally involves the dorsal aspect of the brain stem. The Sonic-Hedgehog (SHH) type (30%) with a 5-year survival of up to 87% depends on the TP53 mutation. Group 3 (25%) with 5-year survival of 32% has the worst prognosis. Group 4 is the most common (35-40%), with 5-year survival of 76% (8, 12, 36-39).

Imaging findings

In CT, medulloblastoma typically appears as a homogeneous mass located near or in the midline, with well-defined contours, with medium to high density compared to the adjacent cerebellar parenchyma, with peritumoral vasogenic edema that, after contrast medium administration, enhances in a diffuse homogeneous or heterogeneous manner. Calcifications can be found in up to 20% of cases and areas of cystic necrosis that do not enhance in up to 50% of cases; intratumoral hemorrhage is rare (17, 34, 36).

In MRI the appearance of medulloblastoma is variable, they can be observed as rounded masses slightly lobulated, with medium or low signal with T1 information, of heterogeneous signal in T2, the solid portion frequently has low to medium signal compared with the cerebellar parenchyma. They usually enhance with the administration of contrast medium, although in a variable way (34, 36, 37) (figure 5).

In spectroscopy sequences they show increased choline peak with decreased NAA and myoinositol peak. Short TE sequences show increased taurine by 3.36 ppmfor increased cell proliferation (12, 22, 36).

In the diffusion sequence, medulloblastomas show high signal in diffusion imaging and low signal in ADC, with low values of diffusion velocity, secondary to the high cellularity of the tumor that decreases the interstitial space and reduces water diffusion (40-45) (Figure 5).

The perfusion sequence shows an increase in relative cerebral blood volume (rCBV) with an average value of 2, in the range of high-grade gliomas (11-5.3) (46). The circulation curve of the contrast medium shows rupture of the blood-brain barrier with accumulation in the extracellular matrix, rather than neoangiogenesis exceeding the baseline (41, 46).

2.2.2. Pilocytic astrocytoma

Cerebellar astrocytoma is the most frequent posterior fossa tumor in children and accounts for approximately 30-35% of cases. It has a peak incidence between the ages of 5-13 years and affects boys and girls equally. Pilocytic astrocytoma is rare in adults, with an incidence of less than 0.1 × 100,000 inhabitants, it occurs in those over 45 years of age, predominantly in the cerebellar hemispheres. It has a very non-aggressive behavior with slow growth, and is classified as grade I astrocytoma by the WHO (5, 12, 34, 47, 48). The classic appearance in the cerebellum is that of a cystic tumor with a hypercapillary mural nodule; there is a solid-cystic form -the most frequent-, but it predominates in the other locations and the solid variant -the least frequent-, predominates in the optic nerve (49).

Imaging findings

In CT it is observed as a predominantly cystic mass in the vermis or cerebellar hemispheres, with a solid area of low density. Occasionally it shows calcifications and hemorrhage is rare (34, 50).

In T1-weighted MRI a cystic lesion of low or slightly high signal to CSF is seen, with solid areas of medium or low signal. On T2-weighted sequences, high-signal solid areas are seen in the gray matter, with medium to high-signal cyst content in the CSF. In FLAIR sequences, high-signal solid areas are seen in the gray matter and the cyst content is not suppressed, so it appears as high signal to the CSF. After the administration of contrast medium, intense enhancement of the solid component is observed (5, 49-51) (Figure 6).

In diffusion sequences the solid portion has diffusion similar to the gray matter with high apparent diffusion coefficients ADC. The

ADC never shows diffusion restriction (17, 21, 50, 52) (Figure 6). Spectroscopy sequences show increased choline with decreased NAA and creatine. Also, lipids and lactate. The choline/NAA ratio is usually elevated (between 1.80 and 3.40) (22, 23, 48, 52).

In perfusion sequences low cerebral blood volume is observed in contrast to the high enhancement after contrast medium administration. Values of rCBV lower than 1.5 and a characteristic curve in the recovery phase of the curve with increased intensity above the baseline are due to loss of contrast medium to the interstitial space and increased permeability (49, 50, 53-55).

2.2.3. Hemangioblastoma

Hemangioblastoma is the most frequent primary posterior fossa tumor in adults, most frequently found in the cerebellum, brainstem and spinal cord. Most are sporadic tumors; however, approximately 25% are familial associated with Von Hippel-Lindau syndrome, typically presenting as multiple hemangioblastomas in young patients. They manifest with signs of endocranial hypertension such as headache, vomiting, ataxia odysmetry (5, 12, 56).

The WHO classifies it as a grade I mesenchymal tumor. These are highly vascular and typically intraaxial, located near the pial surface of the cerebellum and spinal cord. They may have leptomeningeal dissemination to the subarachnoid space as hemangioblastomatosis (12).

The classic appearance is that of an intraaxial mass in the posterior fossa with a cyst and a reinforced mural nodule that contacts the pia mater, with large vessels supplying the mural lesion that present a signal void. The cystic lesion is surrounded by brain parenchyma that may have reactive gliosis without tumor infiltration. Forty percent present as solid nodules without associated cyst. Probably, all hemangioblastomas start as solid nodules frequently small and asymptomatic with vascular hyperpermeability and plasma extravasation with vasogenic edema and cyst formation (5, 12, 57).

Imaging findings

CT shows a low density cystic lesion with a medium density nodule that enhances after the application of contrast medium. Calcifications are extremely rare and may present hemorrhage due to hypervascularity (37, 57-59) (Figures 7 and 8).

In MRI, in T1-weighted sequences, an intermediate signal nodule is seen with the encephalon, flow voids and high light/moderate signal of the cyst compared to the cerebrospinal fluid (CSF). In sequences with T2 information the nodule and cyst have high signal, with prominent flow voids. In FLAIR sequence both the nodule and the cyst are observed with high signal. The nodule enhances intensely with contrast medium, it is rare to observe enhancement of the cyst wall (5, 12,34,60-62) (figures 7 and 8).

In the diffusion sequences high ADC is observed in the cystic and solid portions related to a great amount of capillaries inside the tumor, with values greater than 1 similar to CSF (21 ,42,53) (figures 7 and 8).

In the spectroscopy sequence minimal elevation of the choline peak is observed, lipids can be seen in the cystic portion. In the perfusion sequences a marked increase in cerebral blood volume (rCBV) is observed with an average rCBV value of 26.6 with ranges of 18.34-40.75 and increased permeability (53, 63, 64).

2.2.4. Intraventricular neurocysticercosis (IV ventricle)

Neurocysticercosis (NCC) is the most important helminthic infection of the central nervous system in the world, which occurs when by fecal-oral contamination humans ingest the eggs of Taenia solium and become intermediate hosts; the oncospheres migrate by hematogenous route to various tissues, most frequently to the central nervous system, eyes, muscles and subcutaneous cellular tissue. Once it reaches the neural tissue, the parasite goes through five stages: non-cystic, vesicular, vesicular-colloidal, nodular-granulomatous, and nodular-calcified (65-70). Depending on where the cysticercus lodges, NCC can be parenchymal, subarachnoid, ventricular or medullary. In the intraventricular form, the larva reaches the ventricles via the choroid plexus and causes symptoms due to obstruction of cerebrospinal fluid flow and/or ependymitis (66, 71-73).

Imaging findings

On CT they appear as low density lesions that enlarge the fourth ventricle and cause hydrocephalus. Many have intermediate density to CSF and are only inferred when alteration of the shape of the ventricle is observed, which can be a diagnostic challenge especially if there are no associated calcified parenchymal lesions (74).

In MRI the cysts usually behave with CSF-like signal in T1- and T2-weighted sequences. The cyst wall can be seen as a low signal linear structure in T2 sequences or it can show enhancement after contrast medium administration, with deformity or distension of the fourth ventricle associated with hydrocephalus. In FLAIR sequence it can be observed with discrete higher signal compared to CSF. The presence of scolex is seen as an eccentric high signal focus in the cyst, which is considered an absolute criterion for the diagnosis of neurocysticercosis. With contrast medium, enhancement of the cyst wall or ependymal enhancement can be observed if there are associated inflammatory changes (67,68,71,74-77) (Figure 9).

High resolution cisternography sequences improve the visualization of intraventricular cysts, which can demonstrate the scolex. These sequences should always be included when neurocysticercosis is suspected. In spectroscopic sequences NCC behaves similarly to pyogenic abscesses with increased choline, lactate, succinate, alanine, lipids and acetate, with decreased creatine and n-acetylaspartate (78-80).

In the diffusion sequences a signal similar to CSF is observed, with high ADC, which differentiates it from pyogenic abscesses that present diffusion restriction with low ADC. However, when scolex is present, it shows high signal in the diffusion sequence. In perfusion MRI there is no increase of rCBV in the white matter, which reflects the absence of angiogenesis and hyperperfusion (78, 81, 82) (Figure 9).

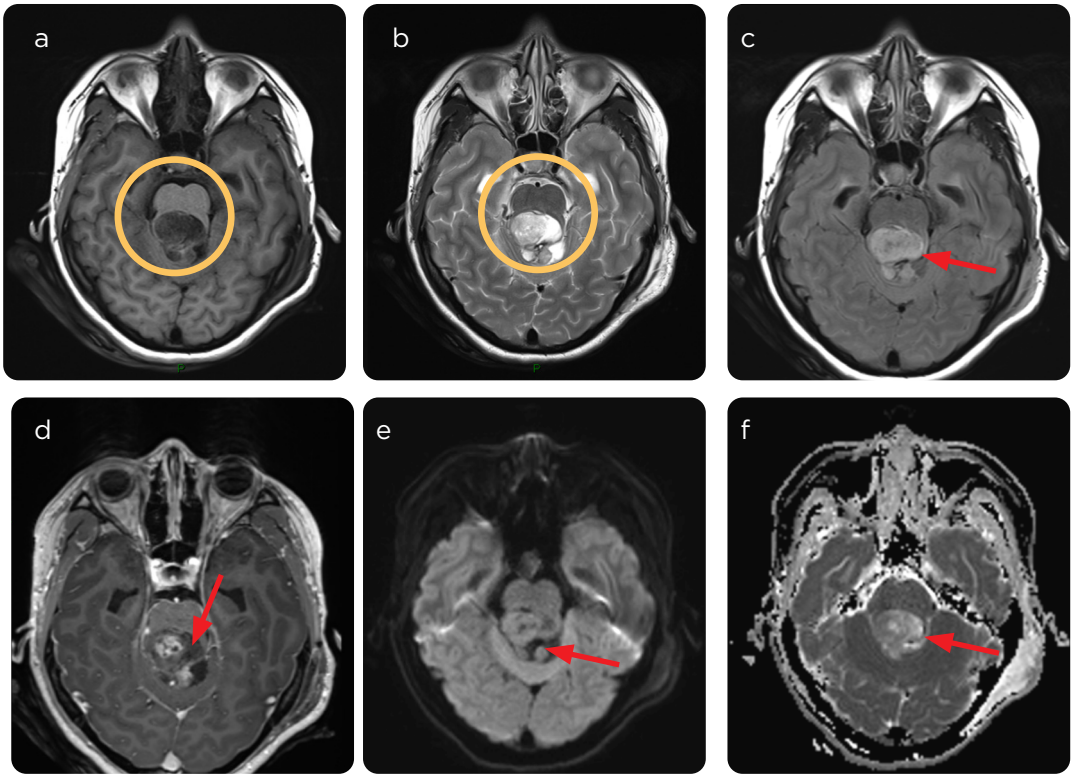

Figure 5. Medulloblastoma. a) MRI with T1 information: low signal. b) Spin echo sequence and c) FLAIR with T2 information: high signal. d) With contrast medium: heterogeneous enhancement. e and f) Diffusion sequences and ADC map: some areas with water diffusion restriction.

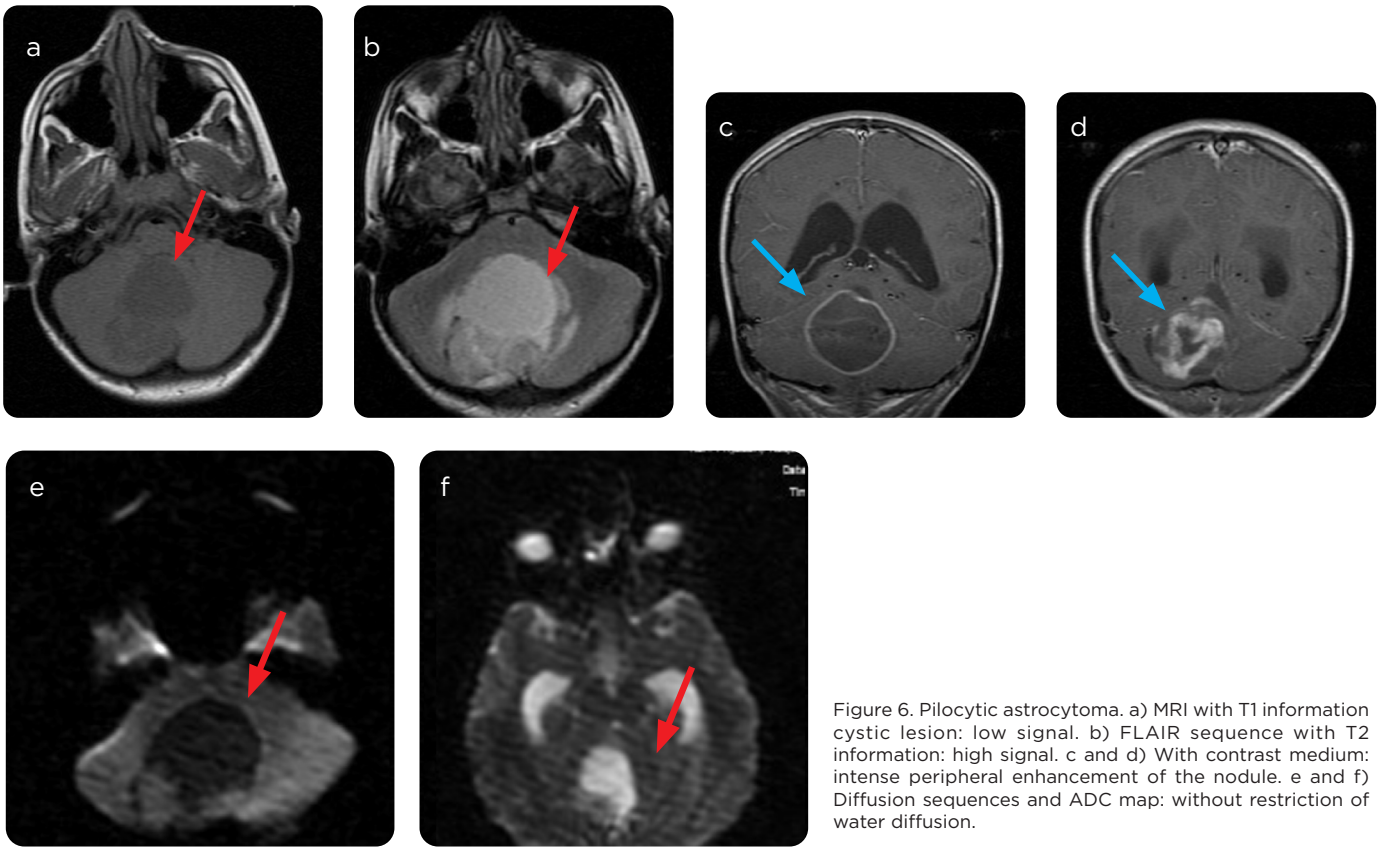

Figure 6. Pilocytic astrocytoma. a) MRI with T1 information cystic lesion: low signal. b) FLAIR sequence with T2 information: high signal. c and d) With contrast medium: intense peripheral enhancement of the nodule. e and f) Diffusion sequences and ADC map: without restriction of water diffusion.

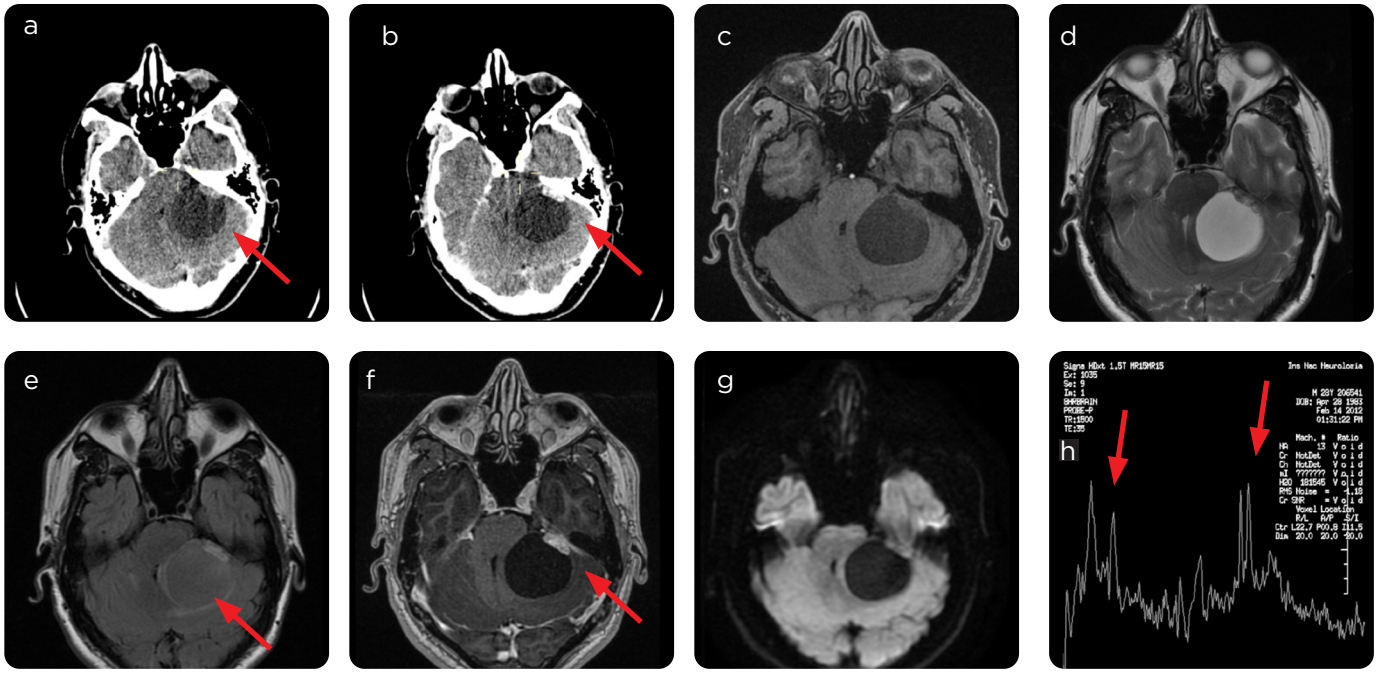

Figure 7. Hemangioblastoma. a) Simple CT and b) with contrast medium: low density lesion well delimited in the left cerebellar hemisphere, with compression of the fourth ventricle. c) MRI sequence with T1 information: low signal. d) Sequences with T2 information: high signal. e) FLAIR sequence: partial suppression of the signal. f) With contrast medium: mural nodule that enhances homogeneously with gadolinium. g) Diffusion sequence: no restriction to water diffusion. h) Spectroscopy: slight increase of the choline peak and increase of the lipid peak in the cystic portion.

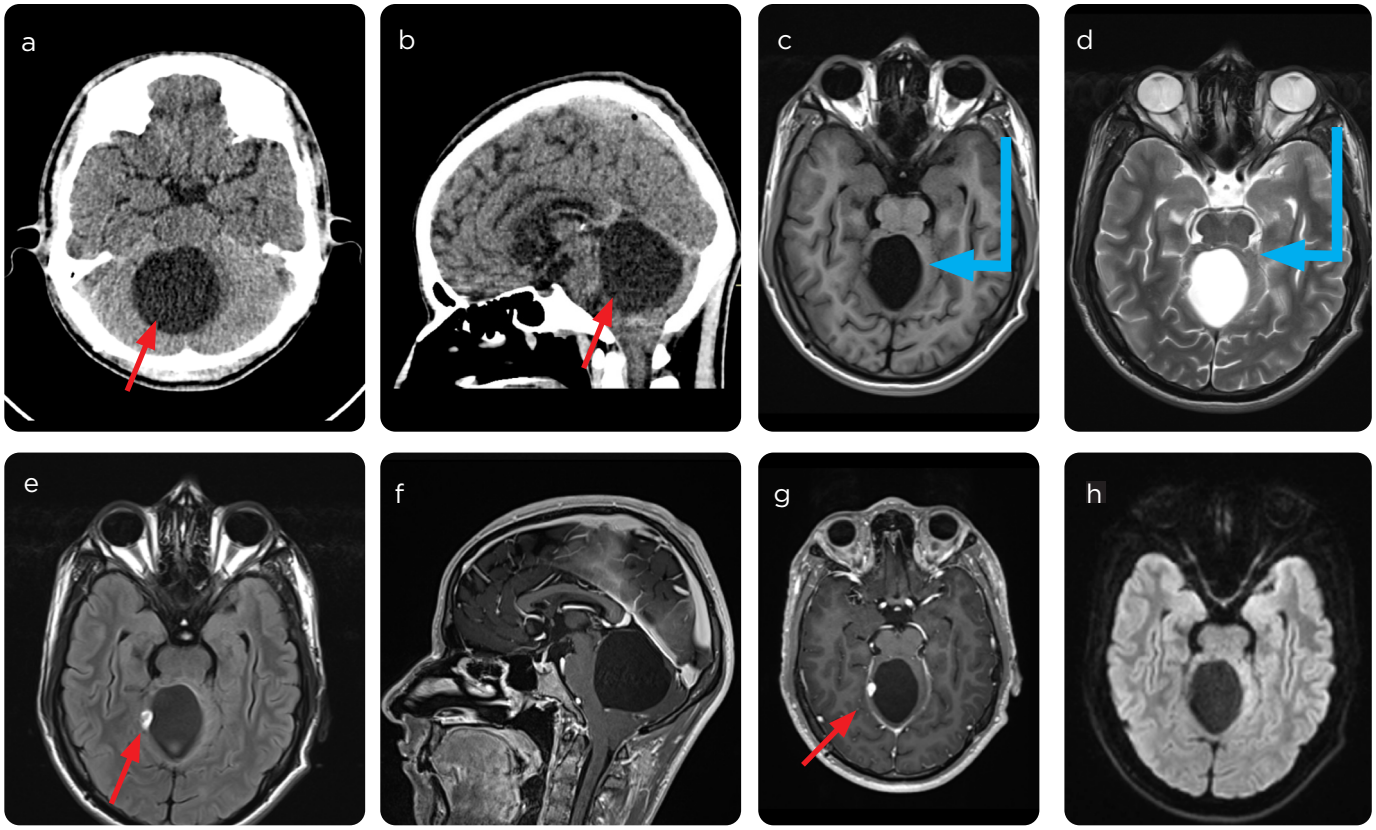

Figure 8. Hemangioblastoma. a) Axial and b) sagittal CT: lesion of CSF-like density, well delimited from the cerebellar vermis. c) MR sequences with T1 information: low signal. d) Spin-echo sequences and e) FLAIR with T2 information, high signal with mural nodule of intermediate signal similar to the gray matter. f and g) With contrast medium: homogeneous enhancement. h) Diffusion sequence: no restriction to water diffusion.

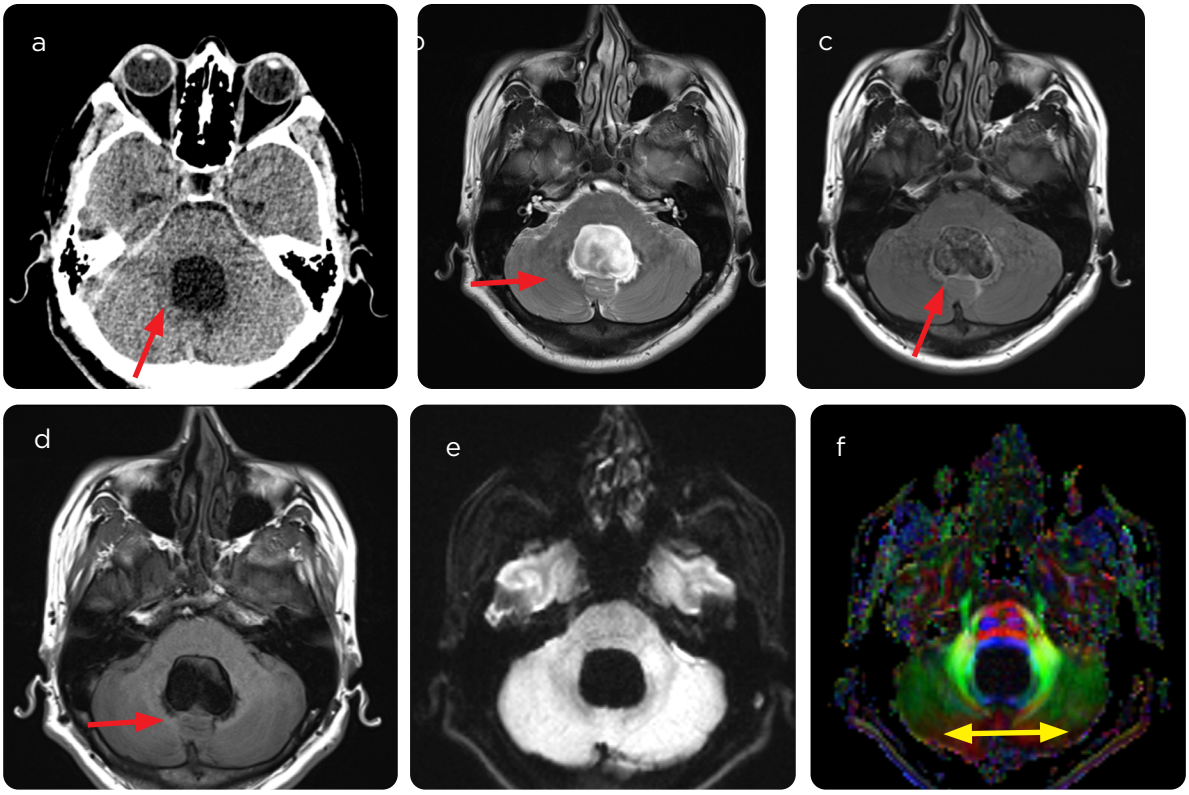

Figure 9. Cysticercus in colloidal vesicular stage occupying the IV ventricle. a) Axial CT scan: CSF-like lesion. b) spin-echo MRI and FLAIR with T2 information: heterogeneous lesion with higher signal and with little perilesional edema. c) Sequence with T1 information: CSF-like signal. d) Diffusion sequence without restriction to diffusion and f) color map tractography: displacement of the white matter tracts adjacent to the cysticercus.

3. Conclusion

Taking into account clinical, demographic data and imaging findings with routine imaging techniques, as well as advanced diffusion, perfusion and spectroscopy techniques, a more accurate diagnosis can be established in the presence of a lesion that primarily or secondarily involves the fourth ventricle.

References

1. Fontana H, Belziti H, Requejo F, Recchia M. Buratti S. Los recesos del IV ventrículo. Rev Argent Neuroc. 2006; 20:101-13.
2. Agarwal A, Kanekar S. Intraventricular tumors. Semin Ultrasound CT MRI. 2016;37:150-8.
3. Koeller K, Sandberg G. Cerebral intraventricular neoplasms: radiologic-pathologic correlation. Radiographics. 2002;(22):1473-505.
4. Smith A, Simirniotopoulos J. Horkanyne-Szakaly I. Intraventricular Neoplasms: Radiologic- Pathologic Correlation. RadioGraphics. 2013;33:21-43.
5. Salgado A, Shehadeh S, Morales E, Santamarta E, Morán M, Saiz A, Oviedo E. Lesiones inusuales de la fosa posterior. Hallazgos de Neuroimagen. S-1299 SERAM.
6. Wolff J, Sajedi M, Brant R, Coppes M, Egeler R. Choroid plexus tumours. Br J Cancer. 2002;87:1086-91.
7. Jusué I, Ortega M, Tamarit M, Poveda P. Papiloma atípico de los plexos coroideos en el adulto: publicación de un caso clínico y revisión de la bibliografía. Neurocirugía. 2012;23(3):116-21.
8. Louis D, Perry A, Reifenberger G, Von Deimling A, Figarella-Branger D, Cavenee W, et al. The 2016 World Health Organization Classification of Tumors of the Central Nervous System: a summary. Acta Neuropathol. 2016;131:803-20.
9. Fenchel M, Beschorner R, Naegele T, Korn A, Ernemann U, Hoger M. Primarily solid intraventricular brain tumors. Eur J Radiol. 2012;81:e688-96.
10. Hernández P, Villanueva M, Vacas M, Sánchez J, Asensio J, Villanueva J. Tumores intraventriculares: Revisión de los hallazgos radiológicos característicos mediante TC y RM convencional. Congreso de la SERAM; 2012, mayo 24-28. Disponible en: https://epos.myesr.org/poster/esr/seram2012/S-1331.
11. Zabala I, Llorente S, Laganâ C, Barbosa del Olmo A, Cigüenza Sancho M, Gordillo Vélez CH. Tumores intraventriculares: Nuevas entidades y hallazgos recientes en resonancia magnética. Congreso de la SERAM; 2014. Disponible en: https://epos.myesr.org/poster/esr/seram2014/S-0546.
12. Shih RY, Smirniotopoulos JG. Posterior fossa tumors in adult patients. Neuroimag Clin N Am. 2016;26:493-510.
13. Bohara M, Baru M, Fujio S, Higashi M, Yonezawa H, Karki P, et al. Choroid plexus tumors: experience of 10 cases with special references to adult cases. Neurol Med Chir. 2015;55:891-900.
14. Krieger MD, Panigrahy A, McComb JG, Nelson MD, Liu X, González-Gómez I, et al. Differentiation of choroid plexus tumors by advanced magnetic resonance spectroscopy. Neurosurgical focus. 2005;15:18(6A).
15. Verma A, Kumar I, Verma N, Aggarwal P, Ojha R. Magnetic resonance spectroscopy — Revisiting the biochemical and molecular milieu of brain tumors. BBA Clinical. 2016;5:170-8.
16. Grossman R, Ram Z. Posterior fossa intra-axial tumors in adults. World Neurosurg. 2016;88:140-5. doi: 10.1016/j.wneu.2015.12.066.
17. Raynaud C, Ramaswamy V, Taylor M, Laughlin S. Posterior fossa tumors in children: Developmental anatomy and diagnostic imaging. Childs Nerv Syst. 2015;31:1661-76.
18. Thompson YY, Ramaswamy V, Diamandis P, Daniels C, Taylor MD. Posterior fossa ependymoma: current insights. Childs Nerv Syst. 2015;31:1699-706.
19. Sayegh ET, Aranda D, Kim JM, Oh T, Parsa AT, Oh MC. Prognosis by tumor location in adults with intracranial ependymomas. J Clin Neurosci. 2014;21(12):2096-101.
20. U-King-Im JM, Taylor MD, Raybaud C. Posterior fossa ependymomas: new radiological classification with surgical correlation. Childs Nerv Syst. 2010;26:1765-72.
21. Olabarria IV, Villanúa JA, Fernández B, Ontañon JM, Cabrera A, Saralegui I. Tumores de fosa posterior y Difusión. Congreso Seram. Granada; 24-28 de mayo de 2012. Disponible en: https://epos.myesr.org/poster/esr/seram2012/S-0891.
22. Brandão LA, Castillo M. Adult brain tumors clinicalapplications of magnetic resonance spectroscopy. Magn Reson Imaging Clin N Am. 2016;24:781-809.
23. Majós C, Aguilera C, Cos C, Camins À, Candiota AP, Delgado-Goñi T, et al. In vivo proton magnetic resonance spectroscopy of intraventricular tumours of the brain. Eur Radiol. 2009;19:2049-59.
24. Kim Y, Lee SY, Yi KS, Cha S, Gang M, Cho B, et al. Infratentorial and Intraparenchymal Subependymoma in the Cerebellum: Case Report. Korean J Radiol. 2014;15(1):151-5.

25. Landriel F, Besada C, Migliaro M, Christiansen S, Goldschmidt E, Yampolsky C, et al. Atypical hemorrhagic presentation of a fourth ventricle subependymoma: Case Report. Neurol Med Chir (Tokyo). 2013;53:828-31.
26. Jain A, Amin AG, Jain P, Burger P, Jallo GI, Lim M, et al. Subependymoma: clinical features and surgical outcomes. Neurol Res. 2012;34(7):677-84.
27. Burguete A. WHO grade I intraventricular tumors: findings in diffusion, perfusion and spectroscopy. Congreso SERAM C-1990. Coruña 2012. Disponible en: https://epos.myesr.org/poster/esr/ecr2012/C-1990.
28. Ragel BT, Osborn AG, Whang K, Townsend JJ, Jensen RL, Couldwell WT. Subependymomas: An analysis of clinical and imaging features. Neurosurgery. 2006;58:881-90.
29. Alver I, Abuzayed B, Kafadar AM, Muhammedrezai S, Sanuz GZ, Akar Z. Primary Fourth Ventricular Meningioma: Case Report and Review of the Literature. Turkish Neurosurgery. 2011;21(2):249-253.
30. Takeuchi S, Sugawara T, Masaoka H, Takasato Y. Fourth ventricular meningioma: a case report and literature review. Acta Neurol Belg. 2012;112:97-100.
31. Khedr S, Hassaan M, Refaat A. The diagnostic value of diffusion weighted imaging in patients with meningioma. Egyptian J Radiol Nuclear Med. 2012;43:249-56.
32. Cabada T, Caballero M, Insausti I, Álvarez de Eulate N, Bacaicoa C, Zazpe I, et al. Papel de la difusión en la evaluacion de los meningiomas: correlación radiopatológica. Radiología. 2009;51(4):411-9.
33. Yin B, Liu L, Zhang B, Li YX, Li Y, et al. Correlating apparent diffusion coefficients with histopathologic findings on meningiomas. Eur J Radiol. 2012;81:4050-6.
34. Poretti A, Meoded A, Huisman T. Neuroimaging of pediatric posterior fossa tumors including review of the literature. J Magnetic Resonance Imag. 2012;35(1):32-47.
35. Coyle B, Kessler M, Sabnis D, Kerr I. ABCB1 in children's brain tumours. Biochem Soc Trans. 2015;43(5):1018-22.
36. Massimino M, Biassoni V, Gandola L, Garrè M, Gatta G, Giangaspero F, et al. Childhood medulloblastoma. Crit Rev Oncol/Hematol. 2016;105:35-51. http://dx.doi.org/10.1016/j.critrevonc.2016.05.012.
37. Bartlett F, Kortmann R, Saran F. Medulloblastoma. Clin Oncol. 2013;25(1):36-45.
38. Taylor M, Northcott P, Korshunov A, Remke M, Cho Y, Clifford S, et al. Molecular subgroups of medulloblastoma: the current consensus. Acta Neuropathol. 2012;123(4):465-72.
39. Northcott P, Korshunov A, Pfister S, Taylor M. The clinical implications of medulloblastoma subgroups. Nat Rev Neurol. 2012;8(6):340-51. doi:10.1038/nrneurol.2012.78.
40. Martínez M. Meduloblastoma pediátrico, revisión y puesta al día. Radiología. 2011;53(2):134-45.
41. Yamashita Y, Kumabe T, Higano S, Watanabe M, Tominaga T. Minimum apparent diffusion coefficient is significantly correlated with cellularity in medulloblastomas. Neurological Research. 2009;31(9):940-6.
42. Abdul Z, Saini J, Ranjan M, Gupta A, Sabharwal P, Purushotham N. Diffusion tensor imaging in evaluation of posterior fossa tumors in children on a 3T MRI scanner. Indian J Radiol Imaging. 2015;25(4):445-52.
43. Pierce T, Kranz P, Roth C, Leong D, Wei P, Provenzale J. Use of apparent diffusion coefficient values for diagnosis of pediatric posterior fossa tumors. Neuroradiol J. 2014;27:233-44.
44. Rodríguez D, Awwad A, Meijer L, Manita M, Jaspan T, Dineen R, et al. Metrics and textural features of MRI diffusion to improve classification of pediatric posterior fossa tumors. Am J Neuroradiol. 2014;35:1009-15.
45. Rumboldt Z, Camacho D, Lake D, Welsh C, Castillo M. Apparent diffusion coefficients for differentiation of cerebellar tumors in children. Am J Neuroradiol. 2006;27:1362-9.
46. Jouanneau E, Guzmán R, Desuzinges C, Frappaz D, Louis-Tisserand G, Sunyach MP, et al. Very late frontal relapse of medulloblastoma mimicking a meningioma in an adult: Usefulness of H-Magnetic resonance spectroscopy and diffusion-perfusion magnetic resonance imaging for preoperative diagnosis: case report. Neurosurgery. 2006;58:789-90.
47. Baker S, Ellison D, Gutmann D. Pediatric gliomas as neurodevelopmental disorders. Glia. 2016;64(6):879-95.
48. Helfferich J, Nijmeijer R, Brouwer O, Boon M, Fock A, Hoving E, et al. Neurofibromatosis type 1 associated low grade gliomas: A comparison with sporadic low grade gliomas. Critical Rev Oncol/Hematol. 2016;104:30-41.
49. Arango J, Menor F, Viguer R, Esteban M, Palacios P, Assing O. Astrocitoma pilocítico pediátrico. Aproximación diagnóstica con TC y RM. Congreso de la SERAM 2012. Disponible en: https://epos.myesr.org/poster/esr/seram2012/S-0744.
50. Gaudio S, Martucci M, Russo R, Visconti E, Gangemi E, D'Argento F, et al. MR imaging of brain pilocytic astrocytoma: beyond the stereotype of benign astrocytoma. Childs Nerv Syst. 2017;33(1):35-54.
51. Collins V, Jones D, Giannini C. Pilocytic astrocytoma: pathology, molecular mechanisms and markers. Acta Neuropathol. 2015;129:775-88.
52. Docampo J, González N, Muñoz A, Bruno C, Morales C. Astrocitoma pilocítico. Formas de presentación. Rev Argent Radiol. 2014;78(2):68-81.
53. Brandão L, Shiroishi M, Law M. A Multimodality approach with diffusion- weighted imaging, diffusion tensor imaging, magnetic resonance spectroscopy, dynamic susceptibility contrast and dynamic contrast-enhanced magnetic resonance imaging. Magn Reson Imaging Clin N Am. 2013;21(2):199-239.
54. Grand S, Kremer S, Tropres I, Hoffmann D, Chabardes S, Lefournier V, et al. Perfusion-sensitive MRI of pilocytic astrocytomas: initial results. Neuroradiology. 2007;49(7):545-50.
55. Uematsu H, M Maeda. Double-echo perfusion-weighted MR imaging: basic concepts and application in brain tumors for the assessment of tumor blood volume and vascular permeability. Eur Radiol. 2006;16(1):180-6.
56. Findeis-Hosey JJ, McMahon KQ, Findeis SK. Von Hippel–Lindau Disease. J Pediatr Genet. 2016;5(2):116-23. http://dx.doi.org/ 10.1055/s-0036-1579757.
57. Schunemann V, Huntoon K, Lonser RR. Personalized medicine for nervous system manifestations of von Hippel–Lindau Disease. Front Surg. 2016;3:39.
58. Wang Z, Hu J, Xu L, Malaguit J, Chen S. Intratumoral hemorrhage in a patient with cerebellar hemangioblastoma a case report and review. Medicine (Baltimore). 2015;94(4):e497.
59. Osorio D, Guevara J. Diagnóstico de hemangioblastoma por tomografía computarizada. Concordancia interobservador. Rev Med IMSS. 2002;40(5):393-7.
60. Arora R. Imaging spectrum of cerebellar pathologies: A pictorial essay. Pol J Radiol. 2015;80:142-50.
61. Leung R, Biswas S, Duncan M, Rankin S. Imaging features of von HippelLindau Disease. RadioGraphics. 2008;28:65-79.
62. Raz E, Zagzag D, Saba L, Mannelli L, Paolo P, Ambrosio F, et al. Cyst with a mural nodule tumor of the brain. Cancer Imaging. 2012;12:237-44.
63. Guan T, Pancharatnam D, Chandran H, Hooi T, Kumar G, Ganesan D. Infratentorial benign cystic meningioma mimicking a hemangioblastoma radiologically and a pilocytic astrocytoma intraoperatively: a case report. J Medical Case Reports. 2013;7:87.
64. Cho S, Na D, Ryoo J, Roh H, Moon C, Byun H, et al. Perfusion MR Imaging: Clinical utility for the differential diagnosis of various brain tumors. Korean J Radiol. 2002;3:171-9.
65. Jensen T, Post J. Intraventricular neurocysticercosis: Presentation, diagnosis and management. Asian Pacific Journal of Tropical Medicine. 2016;9(8):815-8. http://dx.doi.org/10.1016/ j.apjtm.2016.06.016
66. Sinha S, Sharma B. Intraventricular neurocysticercosis: a review of current status and management issues. Br J Neurosurg. 2012;26(3):305-9.
67. Kimura ET, Higuera JA, Corona R, Chávez L, Perochena A, Quiroz L, et al. Neurocysticercosis: Radiologic-Pathologic Correlation. RadioGraphics. 2010;30(6):1705-19.
68. Sarria S, Frascheri L, Siurana S, Auger C, Rovira A. Neurocisticercosis. Hallazgos radiológicos. Radiología. 2013;55(2):130-41.
69. Del Brutto OH. Neurocisticercosis: actualización en diagnóstico y tratamiento. Neurología. 2005;20(8):412-8.
70. Shih R, Koeller K. Bacterial, fungal, and parasitic infections of the central nervous system: Radiologic-pathologic correlation and historical perspectives. RadioGraphics. 2015;35:1141-69.
71. Sánchez A, Monteagudo M, Lozano E, García J. Neurocisticercosis racemosa subaracnoidea gigante y ventricular: a propósito de un caso. Rev Argent Microbiol. 2015;47(3):201-5.
72. Teerasukjinda O, Wongjittraporn S, Tongma C, Chung H. Asymptomatic giant intraventricular cysticercosis: A Case Report. Hawaii J Med Public Health. 2016;75(7):187-9.
73. Matushita H, Campos F, Dante D, Jacobsen M. Hydrocephalus in neurocysticercosis. Childs Nerv Syst. 2011;27(10):1709-21.
74. Del Brutto OH. Neurocysticercosis. The Neurohospitalist. 2014;4(4):205-12.
75. Del Brutto OH. Neurocysticercosis: A Review. Scientific World J. 2012;2012:1-8. https://doi.org/10.1100/2012/159821.
76. Lucato L, Guedes M, Sato J, Bacheschi L, Machado L, Leite C. The role of conventional MR imaging sequences in the evaluation of neurocysticercosis: impact on characterization of the scolex and lesion Burden. Am J Neuroradiol. 2007;28(8):1501-4.
77. Delgado R, Boleaga B, Salgado P. Magnetic resonance imaging in neurocysticercosis. Top Magn Reson Imaging. 2014;23:191-8.
78. Lerner A, Shiroishi M, Zee C, Law M, Go J. Imaging of neurocysticercosis. Neuroimag Clin N Am. 2012;22:659-76.
79. Carpio A, Fleury A, Hauser WA. Neurocysticercosis Five new things. Neurol Clin Pract. 2013;3(2):118-25.
80. Brandao MD, Lara A, Domingues RC. MR spectroscopy of the brain. Philadelphia, PA: Lippincott Williams & Wilkins; 2004.
81. Raffin L, Bacheschi L, Machado L, Nóbrega J, Coelho C, Leite C. Diffusion-Weighted MR imaging of cystic lesions of neurocysticercosis. Arq Neuropsiquiatr 2001;59(4):839-42.
82. Santos G, Leite C, Machado L, McKinney A, Lucato L. Reduced diffusion in neurocysticercosis: Circumstances of appearance and possible natural history implications. Am J Neuroradiol. 2013;34(2):310-6.

Correspondence

Carlos Andrés Arias Durán
Conjunto Mirador de Versalles, torre 4, apartamento 1213
Floridablanca, Santander
cariasduran6@gmail.com

Received for evaluation: June 10, 2020
Accepted for publication: July 29, 2020